Biosensors and Bioelectronics 41 (2013) 621–626

Contents lists available at SciVerse ScienceDirect

Biosensors and Bioelectronics

journal homepage: www.elsevier.com/locate/bios

Reduced graphene oxide field-effect transistor for label-free femtomolar protein detection

Duck-Jin Kim [a], Il Yung Sohn [a], Jin-Heak Jung [b], Ok Ja Yoon [a], N.-E. Lee [a,b,*], Joon-Shik Park [c]

[a] Department of Advanced Materials Science & Engineering, Sungkyunkwan University, Suwon, Gyeonggi-do 440-746, Korea
[b] Department of Advanced Materials Science & Engineering, SKKU Advanced Institute of Nanotechnology (SAINT) and Samsung Advanced Institute for Health Sciences and Technology (SAIHST), Sungkyunkwan University, Suwon, Gyeonggi-do 440-746, Korea
[c] Smart Convergence Sensor Research Center, Korea Electronics Technology Institute (KETI), Seongnam, Gyeonggi-do 463-816, Korea

ARTICLE INFO

Article history:
Received 27 July 2012
Received in revised form
20 September 2012
Accepted 21 September 2012
Available online 9 October 2012

Keywords:
Reduced graphene oxide
Field-effect transistor
Biosensor
Immunosensing
Label-free detection

ABSTRACT

We report reduced graphene oxide field effect transistor (R-GO FET) biosensor for label-free ultrasensitive detection of a prostate cancer biomarker, prostate specific antigen/α1-antichymotrypsin (PSA-ACT) complex. The R-GO channel in the device was formed by reduction of graphene oxide nanosheets networked by a self-assembly process. Immunoreaction of PSA-ACT complexes with PSA monoclonal antibodies on the R-GO channel surface caused a linear response in the shift of the gate voltage, $V_{g,min}$, where the minimum conductivity occurs. The R-GO FET can detect protein-protein interactions down to femtomolar level with a dynamic range over 6-orders of magnitude in the $V_{g,min}$ shift as a sensitivity parameter. High association constants of 3.2 nM^{-1} and 4.2 nM^{-1} were obtained for the pH 6.2 and pH 7.4 analyte solutions, respectively. The R-GO FET biosensor showed a high specificity to other cancer biomarker in the phosphate buffered saline solutions as well as in the human serum.

1. Introduction

The ultrasensitive, label-free electrical detection of proteins in living cell systems as well as in physiological fluids using field-effect transistor (FET) biosensors employing nanoscale sensing materials has shown a great promise for researches of proteomics (Ray et al., 2010) and cellomics (Timko et al., 2010; Lin et al., 2010a, 2010b; Wang et al., 2007; Sudibya et al., 2009) as well as the early diagnosis of cancer (Zheng et al., 2005; Stern et al., 2010; Jacobs et al., 2010). Nano-FETs with one-dimensional (1D) Si nanowire (Si-NW) (Timko et al., 2010; Zheng et al., 2005) or carbon nanotube (CNT) (Ray et al., 2010; Jacobs et al., 2010; Vashist et al., 2011) have shown sensitive detection of cancer biomarkers from nanomolar to femtomolar range in human serum (Ray et al., 2010; Timko et al., 2010; Zheng et al., 2005; Jacobs et al., 2010; Vashist et al., 2011) and *in vitro* detection of nanomolar proteins in cell growth systems (Wang et al., 2007; Sudibya et al., 2009). The limit of detection (LOD) with femtomolar concentration of proteins, comparable to that obtained by labeled optical immunoassay (Krishnan et al., 2011), could be obtained with label-free electrical sensing by Si-NW FET without (Zheng et al., 2005) and with (Gong, 2010) electrokinetic focusing. However, the low-cost, scalable, and reliable fabrication of such nanosensors utilizing 1D nanostructures is still limited due to the constraints of nanofabrication (Ray et al., 2010; Jacobs et al., 2010; Vashist et al., 2011).

Recently, two-dimensional (2D) graphene (Rao et al., 2009; Zhu et al., 2010; Avouris, 2010; Allen et al., 2010) or reduced graphene oxide (R-GO) nanomaterials (Zhu et al., 2010; Eda and Chhowalla, 2010; Compton and Nguyen, 2010; Park and Ruoff, 2009; Dreyer et al., 2010; Park et al., 2010) have found widespread applications. Biosensing applications utilizing graphene (Huang et al., 2010; Dong et al., 2010) or R-GO FETs (Stine et al., 2010; He et al., 2010; Mao et al., 2010) were enabled due to their various advantages including ease of fabrication (Zhu et al., 2010; Allen et al., 2010), low noise level in solution (Cheng et al., 2010; Heller et al., 2010a, 2010b), and high sensitivity to biomolecules (Dong et al., 2010; He et al., 2010; Ohno et al., 2009). Reported biosensors using graphene FETs, however, have indicated limited performance in terms of LOD and dynamic range compared to 1D nano-FETs (Zheng et al., 2005; Stern et al., 2010; Jacobs et al., 2010; Vashist et al., 2011) because polymeric residues generated during transfer of CVD graphene to other substrate or photolithographic patterning hamper surface functionalization and dense immobilization of probe biomolecules on the graphene surface (Yang et al., 2010; Heller et al., 2010a, 2010b).

In nanobiosensors, it was shown theoretically that the larger density of receptor biomolecules on the sensor surface and charges of target analyte biomolecules primarily lower LOD and enhances dynamic range (Heller et al., 2010a, 2010b). In this

* Corresponding author at: Sungkyunkwan University, Department of Advanced Materials Science & Engineering, Suwon-si, Gyeonggi-do, 440-746, Republic of Korea. Tel.: +82 31 290 7398; fax: +82 31 290 7410.
E-mail address: nelee@skku.edu (N.-E. Lee).

0956-5663/$ - see front matter © 2012 Elsevier B.V. All rights reserved.
http://dx.doi.org/10.1016/j.bios.2012.09.040

respect, we believe that R-GO networked films are of great possibility in ultrasensitive biosensing due to no necessity of transfer process resulting in clean surface as well as possibility of facile solution-based fabrication process. It was shown that R-GO nanosheet networked films could be used as an alternative sensing channel of the FET structure for detection of picomolar nucleic acids (Dong et al., 2010), nanomolar antigens with labeling (Mao et al., 2010), and millimolar catecholamines (He et al., 2010). However, detailed investigation on performance factors such as LOD, sensitivity and dynamic range has not been reported during protein detection by using R-GO FETs. Furthermore, a full understanding of the sensing mechanism in R-GO FET biosensors is still lacking (Stine et al., 2010; He et al., 2010; Mao et al., 2010).

Herein, we describe the scalable and facile fabrication of reduced graphene oxide FETs (R-GO FETs) with the capability of the label-free, ultrasensitive electrical detection of proteins, the prostate specific antigen/α1-antichymotrypsin (PSA-ACT) complex biomarker, as an example, in which an ultrathin R-GO channel was formed by the uniform self-assembly of two-dimensional R-GO nanosheets on an aminated substrate. The sensing analyses showed a linear shift in the gate voltage $V_{g,min}$, where the minimum conductivity occurs, with the analyte concentration, a limit of detection as low as 100 fg/ml (~1.1 fM) and wide dynamic range of up to 10^6 in the 1 μM buffer solution. Immunosensing in human serum showed the same LOD of 100 fg/ml but reduced the upper detection limit to 10 ng/ml from 100 ng/ml. The ultrasensitivity having the LOD as low as fM range and the large dyanmic range are presumably attributed to dense immobilization of receptor biomolecules and negligibly small non-specific binding.

2. Material and methods

2.1. Chemicals

3-aminopropyltrimethoxysilane (APTMS), ethanolamine, hydrazine monohydrate, sodium cyanoborohydride and phosphate buffered saline (PBS) solution were purchased from Sigma-Aldrich. 1-pyrenebutanoic acid succinimidyl ester was purchased from Invitrogen. PSA monoclonal antibody (mAb) and PSA-ACT complex were purchased from the Fitzgerald. Amicon Ultra-15 Centrifugal filter device was purchased from the Millipore for desalting of human serum.

2.2. Preparation of GO dispersions

GO nanosheets were synthesized by a modified version of Hummer's method (Park et al., 2008, Yoon et al., 2011). The size of the GO nanosheets was reduced by the sonication in order to enhance the interconnectivity of the fabricated GO films. The GO dispersion in DI water at a concentration of 1 mg/ml was sonicated at a power of 150 W for 24 hrs. Then, the GO dispersion was centrifuged at 4,000 rpm for 1 h to remove the large size GO nanosheets. After this process, the average size of the GO nanosheets was from 500 nm to 1 μm with ~1.2 nm thickness. AFM image of typical GO nanosheets on the Si substrate and line scan across GO nanosheets indicated formation of single-layered GO nanosheets (see Fig. S1 in the Supporting Information). The supernant solution was dialyzed by a 12 K membrane for 1 week to eliminate the residual salt and acids and, in turn, to minimize the agglomeration of the GO nanosheets.

2.3. Fabrication of R-GO FET devices

Fig. 1a–d illustrates the schematic process of device fabrication. The glass substrate was cleaned successively by acetone, alcohol, and DI water. After drying the substrate under nitrogen, sulfuric acid solution with hydrogen peroxide (ratio of H_2SO_4/H_2O_2 of 7:3) was used to make hydroxyl groups on the surface of the glass substrate. After washing with DI water and drying with nitrogen, the substrate was treated by oxygen plasma at a power of 500 W for 10 min to form more hydroxyl groups on the glass surface in preparation for the effective formation of the amine-SAM on the glass substrate. For the selective formation of the sensing channel in the R-GO FET immunosensor, 12.5 wt% solution of (3-aminopropyl)trimethoxysilane (APTMS) in EtOH was treated on the hydroxylated glass surface (Fig. 1a). After 1 h of treatment, the remaining APTMS molecules were washed off by EtOH and heated at 120 °C for 30 min in a nitrogen environment in order to make the surface smooth. And the aminated substrate was immersed into the GO solution for 4 h. The negatively charged GO nanosheets strongly bind to the positively charged surface of the aminated substrate by electrostatic attraction. A study on zeta potentials of GO nanosheets carried out by Li et al. showed the negative potential, i.e. negative surface charges, in water (pH 5.6) as a result of ionization of the carboxylic acid and phenolic hydroxyl groups (Li et al., 2008). And a study on zeta potentials of aminated substrates indicated the positive charges

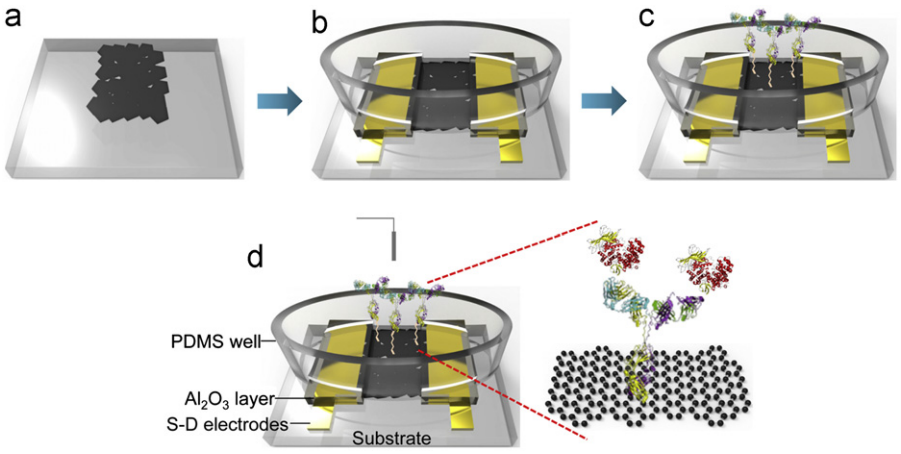

Fig. 1. Schematic of R-GO FET fabrication and detection of PSA-ACT complex. (a) Self-assembly of GO nanosheets on amine SAM substrate and reduction to R-GO. (b) Formation of Ti/Au source and drain electrodes, capping of the electrodes by Al_2O_3 and PDMS layers for minimization of leakage currents. (c) Functionalization of R-GO channel by linker molecules, immobilization of PSA mAb to the linker molecules on R-GO channel, and treatment of ethanolamine (ETA) for non-specific binding. (d) Illustration of R-GO FET immunosensor with Pt reference electrode in the analyte solution. The immunoreactions between antibody (PSA mAb) and the antigen (PSA-ACT complex) caused changes in the carrier density in the R-GO channel due to the doping effects.

of amine groups in water (Kuo et al., 2011). Finally, the self-assembled GO nanosheets were reduced to R-GO by hydrazine vapor for 19 h at 50 °C and annealed for 12 h (For details of selective adsorption of GO nanosheets and reduction, see the Supporting Information).

The Ti/Au source/drain (S/D) electrode and, then, the Al_2O_3 capping layer designed to block the direct interaction of biomolecules with the Au electrodes was selectively formed on the networked R-GO layer by thermal evaporation using a metal shadow mask on the substrate (Fig. 1b). And the PDMS layer was directly pasted on the Al_2O_3 capped S/D electrodes to remove the electrode-electrolyte leakage because photolithographic patterning for encapsulation of electrode induce the photoresist residues which bring about the poor characteristics of immunosensor owing to the disturbance of biomolecule's immobilization (Fig. 1b). Encapsulation of the electrode area by two Al_2O_3 and PDMS layers was important to keep level of the leakage current between the gate and source electrodes undetectable during electrical measurements. The final encapsulation of S/D electrodes defines the sensing area of 100 μm in length and 11,000 μm in width. Finally, the PDMS well was attached to the substrate (Fig. 1b).

The R-GO surface was treated the 10 mM 1-pyrenebutanoic acid succinimidyl ester for 2 h and followed by the PSA monoclonal antibody (PSA mAb) was immobilized to the R-GO (Fig. 1c, also see Supporting Information for detailed immobilization method). Immunosensing characteristics of fabricated R-GO FETs were investigated by measuring their transfer curves (Fig. 1d). The source-drain voltage (V_{sd}) was applied while the electrochemical gate voltage (V_g) was swept by applying a voltage to the Pt reference electrode immersed in the PBS solution containing the PSA-ACT complex analyte molecules (see Supporting Information for detailed characterization method).

3. Results and discussion

3.1. Immunosensing in R-GO FET

Changes in the surface topography were analyzed by atomic force microscopy (AFM) during PSA mAb immobilization on R-GO surface and chemical binding of PSA-ACT complex with the immobilized PSA mAb. AFM results indicated an uniform, well-adhered, well-interconnected and ultrathin R-GO channel with thickness range of single- to bi-layer could be selectively formed on the amine-self assembly monolayer (SAM) substrate from the manufactured GO nanosheets (for details, see the Supporting Information). The R-GO networked films with mono- to bi-layers indicated the room-mean-squared (RMS) roughness of ~0.46 nm.

The R-GO film functionalized with 1-pyrenebutanoic acid succinimidyl ester as linker molecules shows no significance change in surface topography but indicates a slight increase in the RMS roughness to ~0.57 nm (Fig. 2a). The PSA mAb-linked R-GO surface (Fig. 2b) shows densely distributed, small bright spots indicating the binding of PSA mAb molecules and the increased RMS roughness of ~3.4 nm. No preferential adsorption of PSA mAb at the edges or boundaries of R-GO nanosheets was observed even though surface irregularities with PSA mAb immobilization and binding of PSA-ACT complex were seen. The number density of immobilized PSA mAb on R-GO channel was estimated to be about $2x10^{11}$ cm^{-2}. Once the PSA-ACT complexes are bound to the immobilized PSA mAb in the analyte solution with the concentration of 10 pg/ml, the RMS roughness of the R-GO channel was increased to approximately 3.9 nm (Fig. 2c). Changes in the surface morphology and roughness confirm the dense immobilization of PSA mAb and specific binding of PSA-ACT complexes with PSA mAb on the R-GO nanosheets.

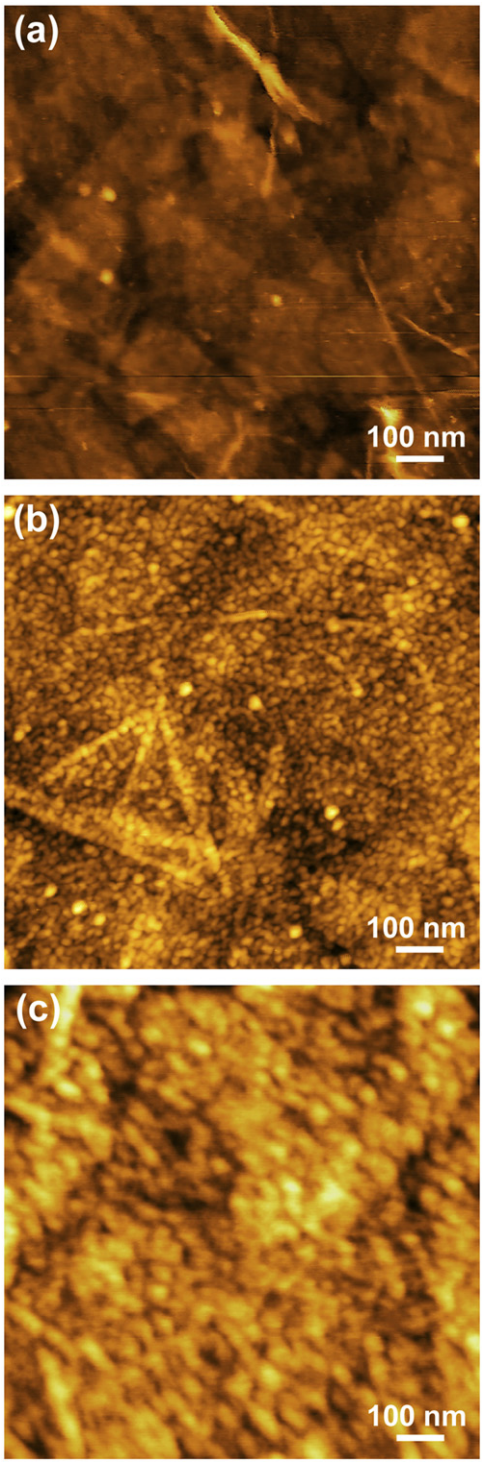

Fig. 2. Surface topography of R-GO channel examined by atomic force microscopy (AFM). (a) R-GO channel surface functionalized by R-GO channel by 1-pyrenebutanoic acid succinimidyl ester as linker molecules. (b) After immobilization of PSA mAb to the linker molecules on R-GO channel, and treatment of ethanolamine (ETA) for non-specific binding. (c) After immunoreactions between antibody (PSA mAb) and the antigen (10 pg/ml concentration of PSA-ACT complex).

Fig. 3a and b show the plots of the channel conductivity, $\sigma(V_g)$, obtained from the R-GO FETs in the 1 μM PBS solutions at pH = 7.4 and 6.2, respectively, with varying analyte concentration, [C] (see the Supporting Information for measurement details). The PBS

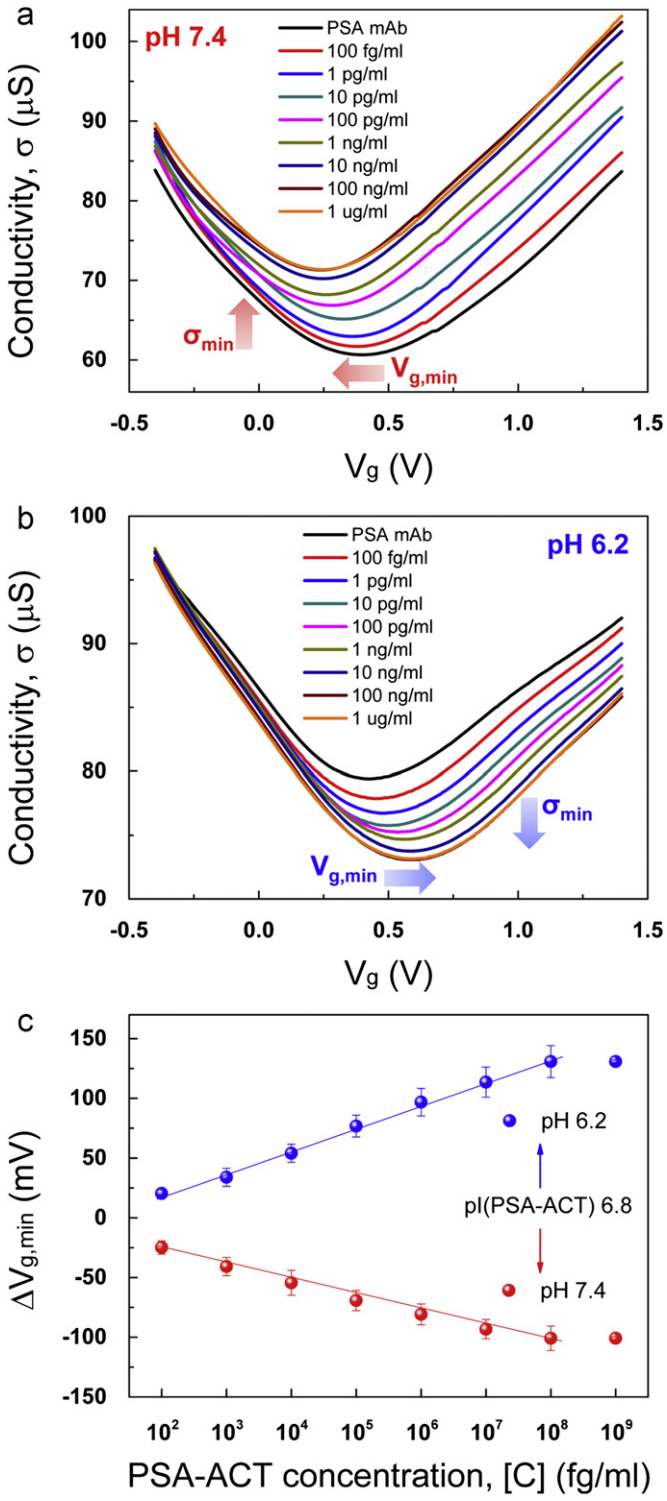

Fig. 3. Detection characteristics of R-GO FET immunosensors. (a–b) $\sigma - V_g$ plot of R-GO FET at a V_{sd} of 0.6 V with various concentrations of PSA-ACT complex in the analyte solutions at (a) pH 7.4 and (b) pH 6.2. (c) Shift in the minimum conductivity point ($\Delta V_{g,min}$) with the concentration of PSA-ACT complex in the pH 7.4 and pH 6.2 analyte solutions. The $\Delta V_{g,min}$ value was obtained by calculating the difference in $V_{g,min}$ as a reference for the device with no binding of PSA-ACT complex.

solutions were diluted to 1 μM concentration, which ensures that charged conjugates of PSA mAb and PSA-ACT complex with the length of ~15 nm are located within the Debye screening length of the PBS solution. The Debye screening length in the 1 μM PBS solution is estimated as 70–80 nm (Stern et al., 2007). The channel conductivity was measured after 10 min on addition of the analyte solutions. To improve the reliability of the measurements of the R-GO FETs, six samples for each pH analyte solution were measured, and the average values and relative standard deviations were analyzed. Since its isoelectric point is 6.8 (Armbruster, 1993), the PSA-ACT complex is negatively and positively charged in the PBS solutions at pH=7.4 and 6.2, respectively. Increasing the analyte concentration, [*C*], by one order of magnitude in the solutions at pH=7.4 (Fig. 3a) and pH=6.2 (Fig. 3b) caused a shift in the gate voltage where the minimum conductivity occurs, $\Delta V_{g,min}$, of -20 ± 4.0 mV and $+20 \pm 4.5$ mV in the negative and positive directions, respectively, giving a sensitivity of -20 ± 4.0 and $+20 \pm 4.5$ mV/decade (Fig. 3c). The use of $\Delta V_{g,min}$ as a sensing parameter indicates that the R-GO FET biosensors for the detection of the PSA-ACT complex are detectable with a large dynamic range with 10^6 and diagnosable down to an extremely low LOD of 100 fg/ml (~1.1 fM), which is similar to the LOD of 90 fg/ml for Si NW-FETs (Zheng et al., 2005) and is smaller than 1 ng/ml for CNT-FETs (Jacobs et al., 2010) fabricated by the bottom-up approach, even though the smaller LODs of 300 aM for surface plasmon resonance (SPR) using superparamagnetic particles (Krishnan et al., 2011) and of 1 aM for Si NW-FET using the preconcentration by using electrokinetics were reported (Gong, 2010).

In addition to the shifts of $V_{g,min}$, a gradual shift in the minimum conductivity σ_{min} at $V_{g,min}$, $\Delta\sigma_{min}$, was observed and the slope of the $\sigma(V_g)$ plots in the region away from the minimum conductivity point was changed with increasing [*C*] (Fig. 3a and b). With increasing [*C*] in the pH 7.4 analyte solution, a positive $\Delta\sigma_{min}/\sigma_{min,0}$, where $\sigma_{min,0}$ is the minimum conductivity with no binding of PSA-ACT complex, was observed (Fig. S9). In the pH 6.2 analyte solution, the tendency was reversed (Fig. S9). The $\Delta\sigma_{min}/\sigma_{min,0}$, however, was not so linear as the $\Delta V_{g,min}$ with varying [*C*]. The change in slope of $\sigma(V_g)$ is related to the change in carrier mobility, μ. The changes in the mobility, $\Delta\mu/\mu_0$, where μ_0 is the carrier mobility with no binding of PSA-ACT complex, were shown in the Fig. S11 (see the Supporting Information for methods of obtaining the μ). Slight increase and decrease in the $\Delta\mu/\mu_0$ for electrons and holes, respectively, were observed with increasing [*C*] in the pH 7.4 analyte solution. The opposite tendencies in the $\Delta\mu/\mu_0$ for electrons and holes observed with increasing [*C*] in the pH 6.8 analyte solution were observed. The observed $\Delta\mu/\mu_0$ with immunoreactions is a result of interplay between inter-sheet hopping of carriers due to nanojunctions (Kobayashi et al., 2010) and intra-sheet hopping of carriers due to potentials induced by attachment of PSA-ACT molecules (Wang et al., 2008).

The negative $V_{g,min}$ shift, i.e. the increase in $|V_g - V_{g,min}|$ with increasing [*C*], in the pH 7.4 analyte solution, gives rise to an increase of net carrier density i.e. n-doping effect, while the positive $V_{g,min}$ shift, i.e. the decrease in $|V_g - V_{g,min}|$ with increasing [*C*], in the pH 6.2 analyte solution gives rise to a decrease of net carrier density, i.e. p-doping effect. Observed directions of shifts in the $V_{g,min}$ by charge doping in this experiment are opposite to the expected shift directions by electrostatic gating effect (Dong et al., 2010; Heller et al., 2010a, 2010b; Li et al., 2005; Heller et al., 2008). Similarly to our results, the n-doping during binding of negatively charged PSA antigens with immobilized PSA mAb on In_2O_3 nanowire FETs in pH 7.4 PBS solution was reported (Li et al., 2005). And interactions of negatively charged DNA molecules (Dong et al., 2010) and positively charged catecholamines (He et al., 2010) with graphene and R-GO surface in FET structures also caused *n*-doping and *p*-doping, respectively.

The mechanisms of these shifts were previously explained based on direct charge transfer doping effects through π–π interactions of analyte biomolecules with surfaces of graphene or R-GO surfaces (Dong et al., 2010; He et al., 2010). However,

a theoretical investigation on interaction of single-stranded DNAs with graphene surface contradicted the direct charge transfer mechanism because the charges transferred to the graphene was not enough to induce the observed charge neutrality point shift due to the weak π–π interaction (Lin et al., 2010a, 2010b). In biosensing utilizing protein-protein interactions, the direct charge transfer from the analyte through the receptor and linker molecules to the sensing surfaces seems to be implausible due to no direct binding of the charged analytes as well as quite a large distance between the charged analytes and R-GO surface. There are also other contradicting results on the shift direction of $\sigma(V_g)$ indicating the *p*-doping, expected from the electrostatic gating effect, by adsorption of negatively charged biomolecules on CNT FETs (Heller et al., 2008) and of negatively charged single-stranded DNAs on graphene FETs (Lin et al., 2010a, 2010b). Furthermore, the charge doping by direct charge transfer or electrostatic gating mechanisms has difficulty in explanation of the changes in $\Delta\sigma_{min}$ and $\Delta\mu$ during biosensing (Dong et al., 2010; He et al., 2010; Lin et al., 2010a, 2010b) in graphene or R-GO FETs.

Alternatively, charge doping induced by charged impurity scattering (Chen et al., 2009a, 2009b, 2008; Das et al., 2008; Adam et al., 2007; Tan et al., 2007; Hwang et al., 2007) rather than by direct charge transfer (Dong et al., 2010; He et al., 2010) or electrostatic gating effect (Heller et al., 2010a, 2010b, 2008) might be presumed. In charged impurity scattering model, the shifts in $V_{g,min}$, σ_{min}, and μ are governed by the charged impurities (Chen et al., 2009a, 2009b, 2008; Das et al., 2008; Adam et al., 2007; Tan et al., 2007; Hwang et al., 2007). Charge transport and doping in the electrochemical gated graphene FETs could be also successfully explained by charged impurity scattering (Chen et al., 2009a, 2009b; Chen et al., 2009a, 2009b). Presence of high density defects and impurities within the R-GO nanosheets and junctions in between R-GO nanosheets, however, lenders theoretical analysis based on the charged impurity scattering model difficult. Understanding of doping mechanism during biomolecular interactions on 2D carbon nanomaterials is still insufficient and requires further study of the mechanism.

3.2. Kinetics study of immunosensing in R-GO FET

In order to explore the reliability of immunosensing by R-GO FET, we investigated the time-dependent conductivity changes for different analyte solutions. The measured data in Fig. 4(a) and (b) for the pH 7.4 and pH 6.2 analyte solutions, respectively, show that the conductivity gradually increases and then almost saturated with the addition of the analyte solutions after about 10 min. Based on the Langmuir model (Halperin et al., 2006), the association constants, K_A, of 3.2 nM^{-1} and 4.2 nM^{-1} were obtained for the pH 6.2 and the pH 7.4 analyte solutions, respectively (see Fig. S12a and b). These values are quite similar to the reported values measured for immunoreactions between PSA mAb and anti-PSA (Lin et al., 2006).

3.3. Specificity test and detection in physiological sample

The specificity of the R-GO FET biosensor for the detection of the PSA-ACT complex was tested with the CEA (carcinoembryonic antigen) biomarker having the isoelectric point of 4.8 (Tu et al., 1998). When the pH 4.2 analyte solution containing CEA markers was applied to the R-GO FET biosensor with the immobilized PSA mAb, no shift of $V_{g,min}$ was observed (Fig. S13a). In the present case, no charge doping contributed to the absence of any shift of $V_{g,min}$. The analyses also indicate that the CEA molecules did not influence the $\Delta\sigma_{min}$ and the change in the $\Delta\mu$ with increasing the CEA concentration. We performed additional experiments to confirm the negligible non-specific binding of the PSA-ACT complexes on the R-GO FETs with no immobilized PSA mAb. The $\sigma(V_g)$

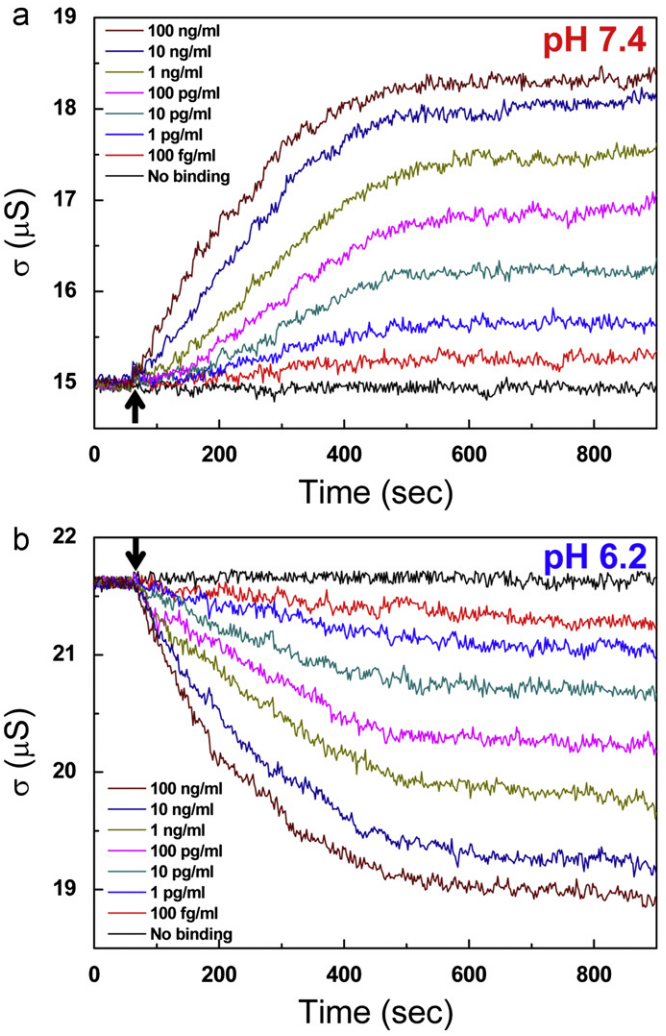

Fig. 4. Electrical conductivity, σ, of R-GO FET immunosensor after the introduction of PBS buffer and analytical solutions containing each concentration of PSA-ACT complex onto the PSA mAb-immobilized R-GO FET at (a) pH 7.4 and (b) pH 6.2. The arrow indicates addition of the analyte solutions. Measurements were carried out at a V_{sd} and V_g of 0.1 and 0.2 V, respectively.

curve measured from the R-GO FET treated by linker molecules, without the immobilization of PSA mAb, in the pH 7.4 analyte solution containing PSA-ACT complexes (Fig. S13b), indicated no charge doping and negligible change in the carrier mobilities in the analyte solution. The analyses also indicated no significant change in the σ_{min}. No significant changes in $\Delta V_{g,min}$, $\Delta\sigma_{min}$ and $\Delta\mu$ upon accumulation of the charged analytes near the R-GO surface without chemical binding cannot be explained by the charged impurity scattering model. These results imply the importance of chemical binding of the charged analytes with the R-GO surface for charge doping.

We further examined the specificity and non-specific binding during immunosensing with mixed analytes of PSA-ACT complex and CEA markers in human serum sample (see Supporting Information for details of measurement). The desalted human serum containg the markers was directly measured by the R-GO FET. The $\Delta V_{g,min}$ of −20 mV was also obtained in human serum similarly to that in the analyte containing PBS solution (Fig. S14). The LOD of PSA-ACT complex was identically 100 fg/ml in both PBS solution and human serum. However, the upper detection limit was reduced from 100 to 10 ng/ml in the human serum sample presumably by increased blocking probability of analyte adsorption due to much higher density of biomolecules near the

R-GO surface in the human serum. The cut-off value of 4 ng/ml suggested for clinical prostate cancer diagnosis is within the dynamic range in the serum (Kim et al., 2010). Even if the physiological solution such as blood and serum has to be desalted or diluted to utilize the reasonable Debye length in FET sensor (Vashist et al., 2011), this biosensor would be possible to detect the extremely small quantity of target protein molecules with high specificity.

4. Conclusions

In summary, the shift of the minimum conductivity point, $V_{g,min}$ caused by the protein-protein interactions on the R-GO FET sensor was linearly correlated with the analyte protein concentration, thus providing a more reliable sensing scheme of proteins in terms of the device parameters in an R-GO FET compared to the shifts of minimum conductivity and the carrier mobilities. 2D self-assembled R-GO film integrated in FET structures can be versatile biosensing materials, due to their ambipolar transport properties associated with charged impurities. R-GO FET devices fabricated by simple, efficient, scalable, low-temperature, and facile solution processes can provide a platform for POC diagnostic systems in future user-friendly health care systems and for ultrasensitive detection of biomolecules *in vitro* or *in vivo* environments.

Acknowledgments

This work was supported by the Basic Science Research Program (Grant no. 2010-0015035) and the WCU Program (Grant no. R32-2008-000-10124-0) through the National Research Foundation of Korea (NRF) funded by the Ministry of Education, Science and Technology (MEST).

Appendix A. Supporting information

Supplementary data associated with this article can be found in the online version at http://dx.doi.org/10.1016/j.bios.2012.09.040.

References

Adam, S., Hwang, E.H., Galitski, V.M., Sarma, S.D., 2007. Proceedings of the National Academy of Sciences, USA 104, 18392–18397.
Allen, M.J., Tung, V.C., Kaner, R.B., 2010. Chemical Reviews 110, 132–145.
Armbruster, D.A., 1993. Clinical Chemistry 39, 181–195.
Avouris, P., 2010. Nano Letters 10, 4285–4294.
Chen, F., Qing, Q., Xia, J., Li, J., Tao, N.J., 2009a. Journal of the American Chemical Society 131, 9908–9909.
Chen, F., Xia, J., Tao, N., 2009b. Nano Letters 9, 1621–1625.
Chen, J.-H., Jang, C., Adam, S., Fuhrer, M.S., Williams, E.D., Ishigami, M., 2008. Nature Physics 4, 377–381.
Cheng, Z., Li, Q., Li, Z., Zhou, Q., Fang, Y., 2010. Nano Letters 10, 1864–1868.
Compton, O.C., Nguyen, S.T., 2010. Small (Weinheim an der Bergstrasse, Germany) 6, 711–723.
Das, A., Pisana, S., Chakraborty, B., Piscanec, S., Saha, S.K., Waghmare, U.V., Novoselov, K.S., Krishnamurthy, H.R., Geim, A.K., Ferrari, A.C., Sood, A.K., 2008. Nature Nanotechnology 3, 210–215.
Dong, X., Shi, Y., Huang, W., Chen, P., Li, L.-J., 2010. Advanced Materials (Weinheim, Germany) 22, 1649–1653.
Dreyer, D.R., Park, S., Bielawski, C.W., Ruoff, R.S., 2010. Chemical Society Reviews 39, 228–240.
Eda, G., Chhowalla, M., 2010. Advanced Materials (Weinheim, Germany) 22, 2392–2415.
Gong, J.-R., 2010. Small (Weinheim an der Bergstrasse, Germany) 6, 967–973.
Halperin, A., Buhot, A., Zhulina, E.B., 2006. Journal of Physics: Condensed Matter 18, S463–S490.
He, Q., Sudibya, G.S., Yin, Z., Wu, S., Li, H., Boey, F., Huang, W., Chen, P., Zhang, H., 2010. ACS Nano 4, 3201 2308.
Heller, I., Chatoor, S., Männik, J., Zevenbergen, M.A.G., Dekker, C., Lemay, S.G.J., 2010a. Journal of the American Chemical Society 132, 17149–17156.
Heller, I., Chatoor, S., Männik, J., Zevenbergen, M.A.G., Oostinga, J.B., Morpurgo, A.F., Dekker, C., Kemay, S.G., 2010b. Nano Letters 10, 1563–1567.
Heller, I., Janssens, A.M., Männik, J., Minot, E.D., Lemay, S.G., Dekker, C., 2008. Nano Letters 8, 591–595.
Huang, Y., Dong, X., Shi, Y., Li, C.M., Li, L.-J., Chen, P., 2010. Nanoscale 2, 1485–1488.
Hwang, E.H., Adam, S., Sarma, S.D., 2007. Physical Review Letters 98, 186806.
Jacobs, C.B., Peairs, M.J., Venton, B.J., 2010. Analytica Chimica Acta 662, 105–127.
Kim, D.-J., Lee, N.-E., Park, J.-S., Park, I.-J., Kim, J.-G., Cho, H.J., 2010. Biosensors and Bioelectronics 25, 2477–2482.
Kobayashi, T., Kimura, N., Chi, J., Hirata, S., Hobara, D., 2010. Small (Weinheim an der Bergstrasse, Germany) 6, 1210–1215.
Krishnan, S., Mani, V., Wasalathanthri, D., Kumar, C.V., Ruslling, J.F., 2011. Angewandte Chemie-International Edition 50, 1175–1178.
Kuo, C.-H., Chang, H.-Y., Liu, C.-P., Lee, S.-H., You, Y.-W., Shyue, J.-J., 2011. Physical Chemistry Chemical Physics 13, 3649–3653.
Li, C., Curreli, M., Lin, H., Lei, B., Ishikawa, F.N., Datar, R., Cote, R.J., Thompson, M.E., Zhou, C.J., 2005. Journal of the American Chemical Society 127, 12484–12485.
Li, D., Müller, M.B., Gilje, S., Kaner, R.B., Wallace, G.G., 2008. Nature Nanotechnology 3, 101–105.
Lin, S., Lee, A.S.-Y., Lin, C.-C., Lee, C.-K., 2006. Current Proteomics 3, 271–282.
Lin, T.-W., Hsieh, P.-J., Lin, C.-L., Fang, Y.-Y., Yang, J.-X., Tsai, C.-C., Chiang, P.-L., Pan, C.-Y., Chen, Y.-Y., 2010a. Proceedings of the National Academy of Sciences, USA 107, 1047–1052.
Lin, Z., Teweldebrhan, D., Ashraf, K., Liu, G., Jing, X., Yan, Z., Li, R., Ozkan, M., Lake, R.K., Balandin, A.A., Ozkan, C.S., 2010b. Small (Weinheim an der Bergstrasse, Germany) 6, 1150–1155.
Mao, S., Lu, G., Yu, K., Bo, Z., Chen, J., 2010. Advanced Materials (Weinheim, Germany) 22, 3521–3526.
Ohno, Y., Maehashi, K., Yamashiro, Y., Matsumoto, K., 2009. Nano Letters 9, 3318–3322.
Park, S., An, J., Piner, R.D., Jung, I., Yang, D., Velamakanni, A., Nguyen, S.T., Ruoff., R.S., 2008. Chemistry of Materials : A Publication of the American Chemical Society 20, 6592–6594.
Park, S., Mohanty, N., Suk, J.W., Nagaraja, A., An, J., Piner, R.D., Cai, W., Dreyer, D.R., Berry, V., Ruoff, R.S., 2010. Advanced Materials (Weinheim, Germany) 22, 1736–1740.
Park, S., Ruoff, R.S., 2009. Nature Nanotechnology 4, 217–224.
Rao, C.N.R., Sood, A.K., Subrahmanyam, K.S., Govindaraj, A., 2009. Angewandte Chemie-International Edition 48, 7752–7777.
Ray, S., Chandra, H., Srivastava, S., 2010. Biosensors and Bioelectronics 25, 2389–2401.
Stern, E., Wagner, R., Sigworth, F.J., Breaker, R., Fahmy, T.M., Reed, M.A., 2007. Nano Letters 7, 3405–3409.
Stern, E., Vacic, A., Rajan, N.K., Criscione, J.M., Park, J., Ilic, B.R., Mooney, D.J., Reed, M.A., Fahmy, T.M., 2010. Nature Nanotechnology 5, 138–142.
Stine, R., Robinson, J.T., Sheehan, P.E., Tamanaha, C.R., 2010. Advanced Materials (Weinheim, Germany) 22, 5297–5300.
Sudibya, H.G., Ma, J., Dong, X., Ng, S., Li, L.-J., Liu, X.-W., Chen, P., 2009. Angewandte Chemie-International Edition 48, 2723–2726.
Tan, Y.-W., Zhang, Y., Bolotin, K., Zhao, Y., Adam, S., Hwang, E.H., Sarma, S.D., Stormer, H.L., Kim, P., 2007. Physical Review Letters 99, 246803.
Timko, B.P., Cohen-Karni, T., Qing, Q., Tian, B., Lieber, C.M., 2010. IEEE Transactions on Nanotechnology 9, 269–280.
Tu, Y.Y., Primus, F.J., Shochat, D., Goldenberg, D.M., 1998. Tumor Biology 9, 212–220.
Vashist, S.K., Zheng, D., Al-Rubeaan, K., Luong, J.H.T., Sheu, F.-S., 2011. Biotechnology Advances 29, 169–188.
Wang, C.-W., Pan, C.-Y., Wu, H.-C., Shih, P.-Y., Tsai, C.-C., Liao, K.-T., Lu, L.-L., Hsieh, W.-H., Chen, C.-D., Chen, Y.-T., 2007. Small (Weinheim an der Bergstrasse, Germany) 3, 1350–1355.
Wang, S., Chia, P.-J., Chua, L.-L., Zhao, L.-H., Png, R.-Q., Sivaramakrishnan, S., Zhou, M., Goh, R.G.-S., Friend, R.H., Wee, A.T.-S., Ho, P.K.-H., 2008. Advanced Materials (Weinheim, Germany) 20, 3440–3446.
Yang, W., Ratinac, K.R., Ringer, S.P., Thordarson, P., Gooding, J.J., Braet, F., 2010. Angewandte Chemie-International Edition 49, 2114–2138.
Yoon, O.J., Jung, C.Y., Sohn, I.Y., Kim, H.J., Hong, B., Jhon, M.S., Lee, N.-E., 2011. Composites: Part A 42, 1978–1984.
Zheng, G., Patolsky, F., Cui, Y., Wang, W.U., Lieber, C.M., 2005. Nature Biotechnology 23, 1294–1301.
Zhu, Y., Murali, S., Cai, W., Li, X., Suk, J.W., Potts, J.R., Ruoff, R.S., 2010. Advanced Materials (Weinheim, Germany) 22, 3906–3924.